Journal of Power Sources 280 (2015) 459–466

Contents lists available at ScienceDirect

Journal of Power Sources

journal homepage: www.elsevier.com/locate/jpowsour

Synthesis of carbon supported ordered tetragonal pseudo-ternary $Pt_2M'M''$ (M = Fe, Co, Ni) nanoparticles and their activity for oxygen reduction reaction

Minh T. Nguyen, Ryo H. Wakabayashi, Minghui Yang, Héctor D. Abruña, Francis J. DiSalvo*

Department of Chemistry, Cornell University, Ithaca, NY 14853-1301, USA

HIGHLIGHTS

- Three ternary ordered intermetallic nanoparticles were synthesized using a novel synthetic method.
- Activity towards oxygen reduction and stability of the catalysts were tested in acidic conditions.
- The catalysts showed comparable to slightly improved activity compared to commercial Pt/C.

ARTICLE INFO

Article history:
Received 3 September 2014
Received in revised form
5 January 2015
Accepted 13 January 2015
Available online 17 January 2015

Keywords:
Ternary intermetallic compounds
PEM fuel cell
Platinum intermetallics
Oxygen reduction reaction

ABSTRACT

Alloying Pt with 3d transition metals has attracted much attention due to their reduced Pt content and reports of enhanced electrocatalytic activity for proton exchange membrane fuel cell applications. However, synthesizing ordered nanocrystalline intermetallics in the sub-10 nm range can be challenging. Here, we report on the co-reduction synthesis of ordered ternary Pt-base transition metal intermetallics with particle sizes in the regime of 3–5 nm. Since differences in the activity of PtM (M = Fe, Co, Ni) for oxygen reduction reaction (ORR) have been reported, we explored their combinations: Pt_2FeCo, Pt_2FeNi, and Pt_2CoNi. These ternary intermetallic nanoparticles crystallized in P4/mmm space group upon annealing in a protective KCl matrix. The electrocatalysts were prepared by dispersing these intermetallics onto a carbon support using ethylene glycol and various sonication techniques. A combination of analytical techniques including powder X-ray diffraction, thermogravimetric analysis, electron microscopy and electrochemical methods have been used in this study. The oxygen reduction reaction activity and stability of the catalysts were tested in 0.1 M $HClO_4$ and 0.1 M H_2SO_4 using cyclic voltammetry and rotating disk electrode voltammetry. The correlations between the composition, structure, morphology and activity of the intermetallics have been established and are discussed.

1. Introduction

Of the different classes of fuel cells, PEMFCs using hydrogen fuel are presently considered the best candidates for automotive applications due to their low operating temperatures, short warm-up time, and acceptable power density. [1–3] In order for commercial implementation of PEMFCs for mobile and transportation applications, the technology needs to be more durable and affordable. [4,5] A major contributor to the high cost is the sluggish kinetics of the oxygen reduction reaction (ORR), which leads to high Pt loadings to reach reasonable power densities. Alloying has been a promising approach to producing advanced catalytic materials. [6–9] It has been shown that alloying Pt with one or more 3d transition metals can not only reduce the Pt content, but also can effectively enhance ORR activity by factor of 2–4 or so by shifting the half-wave potential to more positive potentials by about 30 mV [10–14].

Intermetallics are traditionally synthesized using high temperature reactions and lengthy annealing times. Some common synthetic techniques include arc melting and powder metallurgy, where the reactants are heated to relatively high temperatures (typically above 1000 °C) followed by days or weeks of annealing. [15] Formation of intermetallic phases requires homogenous

* Corresponding author.
E-mail address: fjd3@cornell.edu (F.J. DiSalvo).

http://dx.doi.org/10.1016/j.jpowsour.2015.01.076
0378-7753/

mixing of reactants as small particles (typically 1–100 nm) and high temperatures to overcome the slow solid–solid diffusion rates in the solid state. The lengthy annealing times are necessary for reactants to become homogeneous, nucleating and growing the long range ordered intermetallic structure throughout the material. The high temperature reactions that are required for traditional solid-state synthesis, while important for generating many useful materials, offer little control over morphology and particle size. [16] Thus, synthesizing ordered intermetallic nano-particles (NPs) in the sub 10 nm range can be challenging.

Some methods have been developed to form intermetallic nanocrystals in the 5–10 nm size range. [17–21] For example, Aslam and co-workers have shown that ordered face-centered-tetragonal (fct) PtFe nanocrystals in the 4–6 nm size range can be synthesized by encapsulating alloy PtFe NPs in a SiO_2 shell, which prevents the particles from agglomerating during the annealing at temperatures up to 1000 °C. [22] However, the ordered particles are often kept inside the silica shells, and removal of the silica shells causes the particles to agglomerate. If surface stabilizing surfactants are used during the synthesis, thin carbon layers that are not easily removed, often form during annealing. Sun and co-workers have also shown size controlled PtFe NPs employing a similar method, using MgO to encapsulate the particles and prevent rapid particle growth. [23] MgO is removed with a dilute HCl wash, with only minor Fe metal leaching. However, significant particle agglomeration was observed. Surfactants such as hexadecanethiol and oleic acid are able to stabilize the particles for several hours; however, complete removal of the carbon groups was unable to be achieved. [24] In order to explore the properties of intermetallic nanomaterials as PEMFC catalysis, it is imperative to use a generalizable method of synthesizing well-dispersed, intermetallic nanocrystals with tunable size and composition without the use of strongly coordinating surfactants.

In this paper, we report the synthesis of ordered tetragonal Pt_2FeCo, Pt_2FeNi, and Pt_2CoNi NPs. The co-reduction method (Scheme 1) applied in this study allows the size of the ordered Pt intermetallics to be maintained at 3–5 nm. The ORR activities of these intermetallics on carbon supports were compared to a 50 wt% $Pt/C_{E\text{-}TEK}$ standard.

2. Experimental methods

2.1. Materials

$PtCl_4$ (99.9%, anhydrous), $NiCl_2$ (99.9%, ultra-dry), $CoCl_2$ (99.9% ultra-dry), and LiCl (99.9%, anhydrous) were purchased from Alfa Aesar. $FeCl_3$ (98%, anhydrous), potassium triethylborohydride (1.0 M in THF), and ethylene glycol were purchased from Sigma–Aldrich. Li_6NiCl_8 was synthesized by mixing stoichiometric amounts of $NiCl_2$ and LiCl using a mortar and pestle. The yellow powder was then transferred and sealed in a quartz tube under vacuum and annealed at 540 °C, for 672 h, followed by rapid quench to room temperature. Li_2CoCl_4 was prepared in a similar manner, but annealed at 400 °C for 162 h, then cooled to room temperature naturally. THF and hexanes were dispensed from a custom built Seca solvent system by Glass Contour. All reductions were preformed air-free inside an argon atmosphere glove-box.

2.2. Synthesis of intermetallic NPs

Pt_2FeCo–25KCl: The solvent co-reduction method has been used for the NP synthesis as illustrated in Scheme 1. Briefly, 100 mg of $PtCl_4$ (0.3 mmol), 32 mg of Li_2CoCl_4 (0.15 mmol), 24 mg $FeCl_3$ (0.15 mmol), and 63 mg LiCl (1.5 mmol) were added to a 100 mL three necked round bottom flask and dissolved in 25 mL of dry THF. The solution was then rapidly reduced, via syringe, with 8.5 mL KEt_3BH to account for all the chloride ions in solution with 15 mol% excess. The black solution was then transferred to a 50 mL centrifuge tube, capped with a septum and fastened with copper wire. The solution was spun at 7000 rpm for 5 min and the clear supernatant was removed under a positive pressure of argon and cannula needle. The black precipitate was then washed three times with 30 mL aliquots of dry THF with a final wash with 30 mL of dry hexanes using the above procedure. The black precipitate was then dried under vacuum via schlenk-line. The dried black powder (NPs encased in KCl, NP/KCl) was exposed to air slowly by backfilling the centrifuge tube with Ar, punctured with a needle, and allowed to sit overnight. Similar to the synthesis of Pt_2FeCo–25KCl NPs, Pt_2FeNi–25KCl and Pt_2CoNi–25KCl were synthesized by co-reduction of mixture of $PtCl_4$, Li_6NiCl_8, LiCl and $FeCl_3$ or Li_2CoCl_4, respectively. In order to form ordered intermetallic phases, the NPs/KCl were transferred to a silica tube and sealed under vacuum. The samples

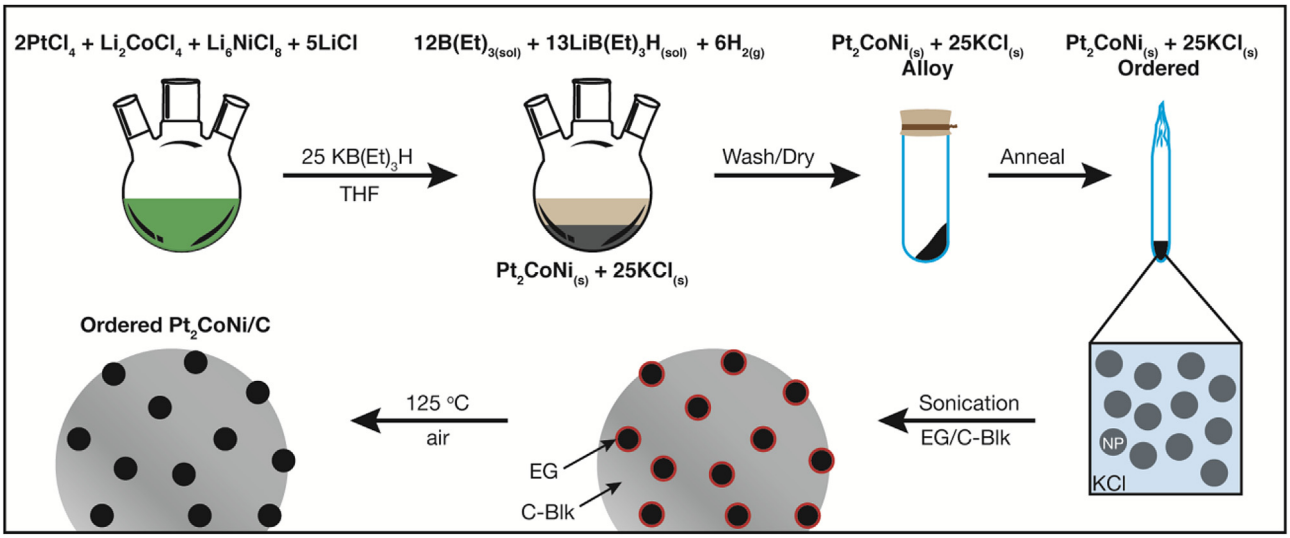

Scheme 1. Co-reduction synthesis of Pt_2CoNi/C catalyst.

were then annealed at 550 °C for 4 h, cooled to 450 °C over 3 h, then held at 450 °C for 15 h, finally cooled to room temperature over 5 h.

2.3. Characterization

The purities of NPs were examined with a Rigaku Ultima VI powder X-ray diffractometer (PXRD) with CuK radiation ($K_{\alpha 1}$, $\lambda = 1.5406$ Å and $K_{\alpha 2}$, $\lambda = 1.5444$ Å). Crystal structures of the NPs were confirmed by PXRD profiles using the GSAS package. [25] The crystalline domain sizes of the NPs can be estimated from a Rietveld fit of the Lorentzian function, as discussed previously. [26] SEM and EDX were performed with a LEO-1550 field emission SEM (FSEM). TEM was performed with a FEI T12 Spirit TEM STEM. The mass percent of NPs on carbon black support was determined using TGA. The samples were heated to 550 °C at a rate of 10 °C/minute, and then held at that temperature until the mass had stabilized for at least 10 min. The measurements were performed under a flow of air to completely oxidize off the carbon support material. Complete oxidation of the non-Pt transition metals is assumed (formation of Fe_2O_3, Co_3O_4, and NiO) and the percent mass difference is subtracted from the experimental value.

2.4. Electrochemical measurements

Transfer of NPs to carbon black (C-Blk) support: 15 mg of C-Blk (Vulcan XC72R, untreated) and 5 mL of ethylene glycol (EG) in a 20-mL scintillation vial, was sonicated (Branson 3510) for 1 h. 26 mg of NPs/KCl with 1.5 mL of EG were ultrasonicated (Microson Ultrasonic Cell Disruptor XL) for 30 s in a 5 mL vial submerged in an ice bath. The NP/KCl/EG solution was then added to C-Blk/EG solution and ultrasonicated for an additional 10 min while submerged in an ice bath. The final solution was centrifuged at 3500 rpm for 20 min. The supernatant was removed and the black precipitate was washed 5 times with 10 mL aliquots of Millipore water. After the final wash, the black precipitate was dried at 125 °C in air for 90 min.

The general procedure for evaluating the electrocatalytic activity of a catalyst involves the casting of a catalyst thin-film of known loading on the surface of a glassy carbon electrode. Glassy carbon electrodes (d = 5 mm) were polished using diamond polishing paste (Buehler) followed by 0.3, and 0.05 μm alumina powder (Extec and Buehler, respectively), rinsed using Millipore water (18 MΩ/cm Millipore Milli-Q) and was sonicated in 1 M NaOH (Maeron, ACS grade) for 5 min to activate the surface. No electrochemical cleaning of the glassy carbon electrodes were performed. Approximately 7 mg of NP/C and 2 mL of 0.02% Nafion solution in ethanol (200 proof, KOPTEC) (so as to make the Pt loading 20 μg/cm^2) was ultrasonicated for several minutes (Microson Ultrasonic Cell Disruptor XL), and 5 μm aliquot was deposited on the electrode. For the Pt_2FeCo/C, Pt_2FeNi/C, and Pt_2CoNi/C catalysts (which are highly hydrophobic), a stock solution of 0.02% Nafion in ethanol was prepared by mixing 0.4 mL of 5 wt% Nafion ionomer solution (Sigma–Aldrich) and 99.6 mL of ethanol in a 100 mL volumetric flask. 2 mL of the stock solution was added to the appropriate amount of NPs/C sample to yield 20 μg/cm^2 loading on the electrode. A 5 μL solution of the ink was drop-cast onto a 5 mm diameter electrode.

Once the thin-film dried, the electrochemical activity was evaluated in a standard three-electrode electrochemical cell with working, counter, and reference electrodes to obtain CVs in a deoxygenated electrolyte using high-purity nitrogen gas (Airgas) and ORR polarization curves in an O_2-saturated (UHP, Airgas) electrolyte.

The electrochemical measurements were done in 0.1 M H_2SO_4 and $HClO_4$ (Alfa Aesar 99.9999%). Pt and Pt-based electrode

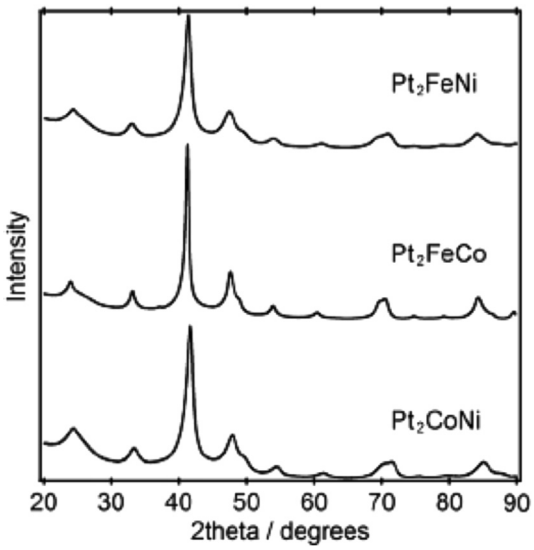

Fig. 1. PXRD patterns of ordered Pt_2FeCo/C, Pt_2FeNi/C and Pt_2CoNi/C made at 550 °C.

catalysts exhibit significantly lower ORR activity in 0.05 M H_2SO_4 compared to $HClO_4$ as the electrolyte. [27,28] This is due to Pt surfaces being highly susceptible to the adsorption of HSO_4^- and SO_4^{2-} ions. For 20 wt% Pt/$C_{E\text{-}TEK}$ standards, mass and specific activities in 0.1 M $HClO_4$ (at 0.9 V scanned at 20 mV/s with a Pt loading of 20 $\mu g_{Pt}/cm^2$) were 0.21 A/mg_{Pt} and 347 $\mu A/cm^2_{Pt}$ respectively, whereas the same electrode under the same conditions in 0.05 M H_2SO_4 electrolyte showed mass and specific activities of 0.07 A/mg_{Pt} and 105 $\mu A/cm^2_{Pt}$ respectively. [29] Despite the lower activities in sulfuric acid electrolytes, we have chosen to carry out the experiments in 0.1 M H_2SO_4 as well. To compare "apples to apples," the results of our catalysts are compared against a Pt/ETEK C-Blk standard under the same conditions.

Cyclic voltammograms (CV) of the catalyst materials were recorded at room temperature between 0.05 and 1.10 V vs. reversible hydrogen electrode (RHE) at a scan rate of 20 mV/s^{-1} using a Bioanalytical Systems CV-27 potentiostat after degassing the electrolyte with N_2 for 20 min prior to the experiment. The ORR activity of the deposited nanomaterials were studied at room

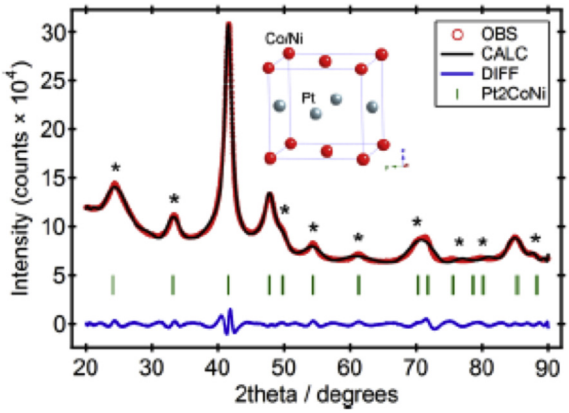

Fig. 2. Sample Rietveld refinement plot of Pt_2CoNi/C. The red pattern is the experimental data. The black line is the calculated pattern. The blue line represents the difference between the calculated and observed patterns. The green tic marks represent the peak locations of tetragonal Pt_2CoNi. The (*) indicates the peaks that appear due to the effects of the ordering of Pt and Fe/Co. (For interpretation of the references to colour in this figure legend, the reader is referred to the web version of this article.)

Table 1
Refinement results of the lattice parameters for the primitive tetragonal unit cell for Pt_2FeCo, Pt_2FeNi, and Pt_2CoNi nanoparticles annealed at 550 °C. The "a-axis" for the "face-centered" unit cells is 3.810, 3.828, and 3.800 Å respectively. As a reference, the unit cell data of Pt is given. Since the a lattice parameters obtained for Pt_2FeCo showed significant deviation from the bulk measurements, we determined the lattice parameters again on a different portion of the sample, obtaining a result that differed by 0.012 Å. The "a" lattice parameter for Pt_2FeCo used in this table and Figs. 3 and 4 is the average of two measurements. Both goodness of fit parameters from two measurements are shown.

Formula	Pt_2FeCo	Pt_2FeNi	Pt_2CoNi	Pt
System	Tetragonal	Tetragonal	Tetragonal	Cubic
Space group	P4/mmm	P4/mmm	P4/mmm	Fm-3m
a, b/Å	2.695	2.706(2)	2.691(2)	3.924(2)
c/Å	3.736(2)	3.673(2)	3.682(2)	3.924(2)
α, β, γ/degree	90	90	90	90
V/Å^3	27.13	26.90(4)	26.67(2)	60.430
Z	1	1	1	4
wR_p	0.0270, 0.0452	0.0573	0.0380	–
R_p	0.0197, 0.0281	0.0432	0.0299	–
Pt–Pt/Å	2.689, 2.695 (2)	2.706(2)	2.691(2)	2.775

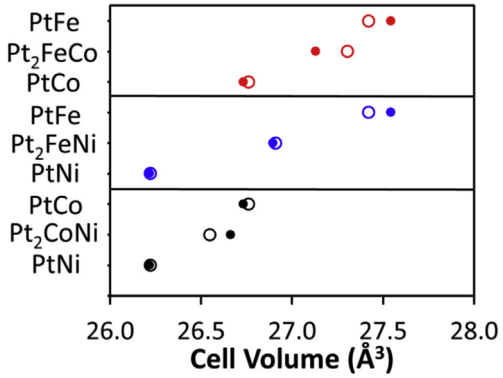

Fig. 3. Plot of bulk and nano cell volumes of PtFe, PtCo, PtNi, Pt_2FeCo, Pt_2FeNi, and Pt_2CoNi. The open circle and solid marks represent the bulk and nano phases, respectively.

temperature via rotating disk electrode (RDE) voltammetry over the potential range of 0.05 and 1.1 V vs. RHE in the negative direction at a scan rate of 20 mV/s[1]. The electrochemical cell was flushed with O_2 for 15 min before the experiment and the flow was maintained over the solution during the course of experiments to assure an O_2 saturated solution. The rotation speed of the disk electrode for all ORR experiments were 1600 rpm. Both CV and RDE experiments were conducted in 0.1M $HClO_4$ and H_2SO_4, where a home-made RHE was used as the reference electrode and a Pt wire as a counter electrode.

The catalysts were subjected to 2000 electrochemical potential cycles from 0.05 to 1.10 V at a rate of 50 mV s^{-1} to examine their stability in terms of real platinum surface area, ORR activity, and the change in composition of Pt and non-Pt metal in the electrode. CVs and RDEs of all the catalysts were recorded after approximately 25 and 2000 cycles. The elemental composition of all the electrodes after the final CV and RDE experiments were measured with EDX. All the potential cycling experiments were carried out at room temperature and ambient pressure.

3. Results and discussion

3.1. Synthesis and crystal structure analysis

The synthesis of Pt-M-M′ NPs was done using a solution phase co-reduction method. The reaction uses metal chloride precursors and sufficient potassium triethylborohydride reducing agent to account for all the Cl^- ions. The NPs prepared at room temperature exhibit a disordered face-centered-cubic structure. The byproduct of the reduction yields metal nanoparticles encased in a KCl "matrix." The KCl serves as a stabilizing agent, allowing formation of the ordered intermetallic phase which adopts a tetragonal structure, via heat treatment at 550 °C, without major agglomeration or increase in particle size. The difference in unit cell and site occupancy of Pt, Co, and Ni atoms of disordered and ordered Pt_2CoNi are given as an example in Fig. S1. A simulated PXRD patterns of disordered and ordered Pt_2CoNi are presented in Fig. S2, which shows the extra diffraction peaks of the ordered phase that arise when transitioning from a disordered face-centered-cubic (fcc) structure to an ordered tetragonal structure on annealing. According to the PXRDs in Fig. 1, all three $Pt_2M'M''$ products, after heat treatment at 550 °C, clearly show the diffraction peaks of the ordered tetragonal phase. The broad hump around 23° (2θ) is the diffraction peak of the carbon black support material. The subtle shifts of the peak positions of the XRD patterns arise from different lattice parameters for the different compositions. The atomic size of Fe, Co, and Ni is 156, 152, and 149 pm respectively. [30] Thus, the lattice parameters are expected to increase in the order of Pt_2CoNi < Pt_2FeNi < Pt_2FeCo. As expected, for example, the (101) peak (the peak at roughly 41° 2θ), shifts to higher angles in the order of Pt_2FeCo < Pt_2FeNi < Pt_2CoNi (an XRD peak shift to higher angles is indicative of smaller lattice parameters). Due to the small domain size of the NPs, the diffraction peaks are relatively broad compared to the PXRDs of bulk samples. [31–33].

Fig. 2 is a representative Rietveld refinement of the pattern from

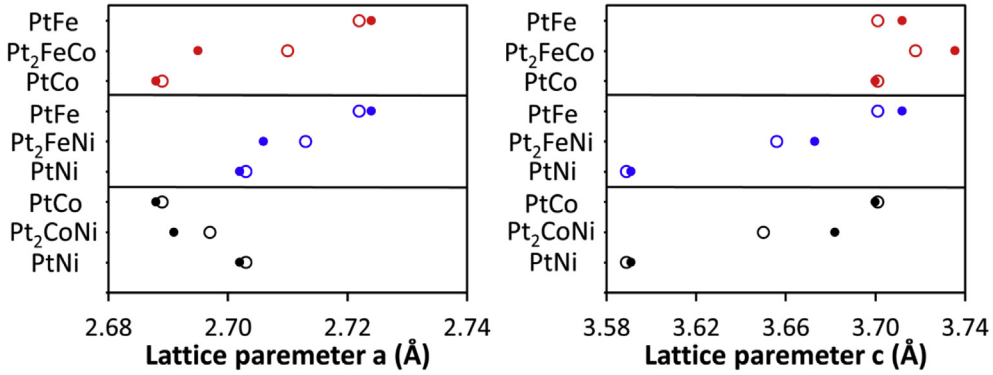

Fig. 4. Lattice parameters (a and c) of bulk and nano PtFe, PtCo, PtNi, Pt_2FeCo, Pt_2FeNi, and Pt_2CoNi materials. The open circle and solid marks represent the bulk and nano phases, respectively.

Pt_2CoNi/C annealed at 550 °C. The Rietveld refinements of the Pt_2FeCo/C and Pt_2FeNi/C are shown in Fig. S3. The refined lattice parameters and other structural information for the Pt_2FeCo/C, Pt_2FeNi/C, and Pt_2CoNi/C samples are summarized in Table 1, and generally agree with the reported lattice parameters of the corresponding bulk materials. [31–33] The Pt–Pt bond distance is equal to lattice parameter a. The refined lattice parameter "a" of Pt_2FeCo, Pt_2FeNi, and Pt_2CoNi are 2.689(2), 2.706(2) and 2.691(2) Å, respectively, which agrees reasonably well with the reported values (2.710(1), 2.713(1) and 2.697(1) Å) of the bulk materials. [31–33] As expected, Pt_2FeCo has the largest unit cell volume of 27.03(1) $Å^3$. The c lattice parameter and cell volume follow the trend expected from the size of the 3d elements; the lattice parameter a, however, does not follow that trend; it is anomalous. This observation may be due to a lattice contraction caused by the strong magnetic moment of Pt_2FeCo (Curie temperature: PtFe > PtCo > PtNi). [31,33] Fig. 3 shows the cell volume of bulk and nano PtFe, PtCo, PtNi, Pt_2FeNi, Pt_2FeCo, and Pt_2CoNi materials. As expected, there is a linear decrease in lattice parameters and volume as the 3d element changes from Fe > FeCo > FeNi > Co > CoNi > Ni among the respective binaries. Fig. 4 shows the lattice parameters (a and c) of bulk and nano Pt_2FeCo, Pt_2FeNi, and Pt_2CoNi alongside their corresponding binary phases. The overall trend in Pt–Pt bond distances (lattice parameter "a") of the pseudo-ternary nanoparticle samples obtained in Table 1 agrees well with the trend observed in the bulk phase (Pt_2FeNi > Pt_2FeCo > Pt_2CoNi).

X-rays are diffracted by the electron density of the atoms. [34] Due to the comparable atomic numbers (electron densities), possible ordering of the Fe/Co/Ni on the 2e Wyckoff position cannot be detected by the X-ray diffraction technique applied in this study. (See Fig. S1 for further information).

3.2. Elemental analysis

Pt, Fe, Co, and Ni atomic percentages of all the catalysts were determined via energy-dispersive X-ray spectroscopy (EDX). At least five different individual spots were selected and measured on each sample. The electron beam is roughly 1 μm in diameter and detects roughly 10^5 - 10^6 particles (assuming a detection sphere of 1 $μm^3$). Fig. S4 shows the EDX spectra of Pt_2FeCo/C, Pt_2FeNi/C, and Pt_2CoNi/C catalysts before ORR testing. These figures also confirm the purity of the products as there are no other elements detected. The atomic compositions of the samples, before and after stability tests, are given in Table S1. Approximately 10 at% of the 3d metal atoms are lost due to leaching after 2000 CV cycles (between 0.05 and 1.10 V at a scan rate of 50 mV/s in 0.1 M H_2SO_4, in a separate experiment). Any exposed 3d metal atoms on the surface of the particles are expected to oxidize and dissolve within the first 2 sweeps; however, typical alloy NPs with initial PtM (M = 3d transition metal) ratios of 50:50 see a reduction of roughly 30 at% of the non-Pt element, stabilizing at the 75–80 atomic at% Pt. [35] Thus, these observations suggest that ordered nanomaterials are chemically and structurally more stable (less prone to leaching) than their alloy counterparts under fuel cell-relevant potential cycling conditions.

The weight % (loading) of the ordered Pt_2FeCo, Pt_2FeNi and Pt_2CoNi NPs on carbon was confirmed by thermogravimetric analysis (TGA). The samples were heated in air from room temperature to 550 °C at 10 °C/min and held at 550 °C to ensure the complete oxidation of carbon. The TGA plots of ordered Pt_2FeCo/C, Pt_2FeNi/C, and Pt_2CoNi/C samples are summarized in Fig. S5. After oxidizing the carbon support material (producing the volatile product CO_2), the percent mass of NPs on carbon was determined to be 26.20%, 25.68%, and 24.04% for Pt_2FeCo/C, Pt_2FeNi/C, and Pt_2CoNi/C, respectively. Correcting for the oxidation of the non-Pt metal (the formation of Fe_2O_3, Co_3O_4, and NiO), the catalyst loadings were determined to be 17.96 wt%, 18.34 wt%, and 17.20 wt% for Pt_2FeCo/C, Pt_2FeNi/C, and Pt_2CoNi/C, respectively. These values compare well with the theoretical loading of 20 wt% as determined by the masses of reactants and carbon black used in the synthesis. This means that >95 wt% of the catalyst is bound to the support and not lost to the supernatant or container walls.

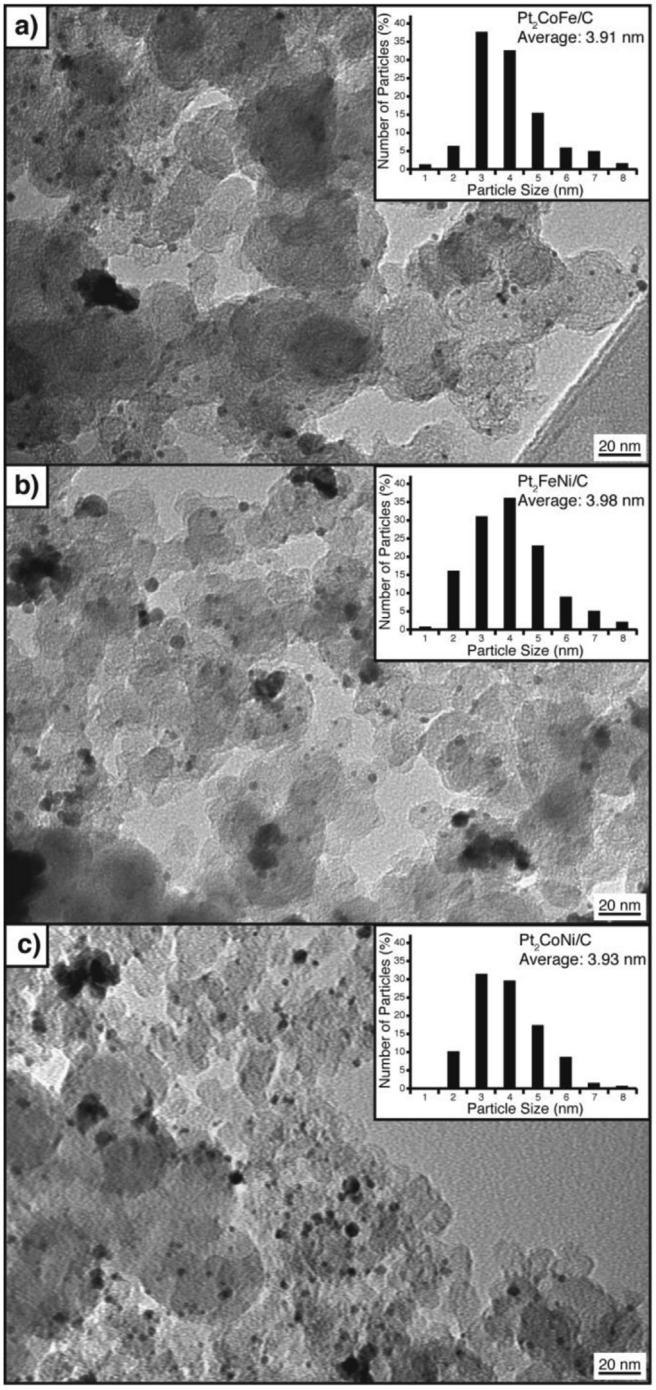

Fig. 5. Particle size histograms (insert) and corresponding TEM image of Pt_2FeCo/C, Pt_2FeNi/C, and Pt_2CoNi/C: The histograms were made by analyzing at least 100 particles and normalized to the total percent of the analyzed particles, ignoring obvious aggregated masses.

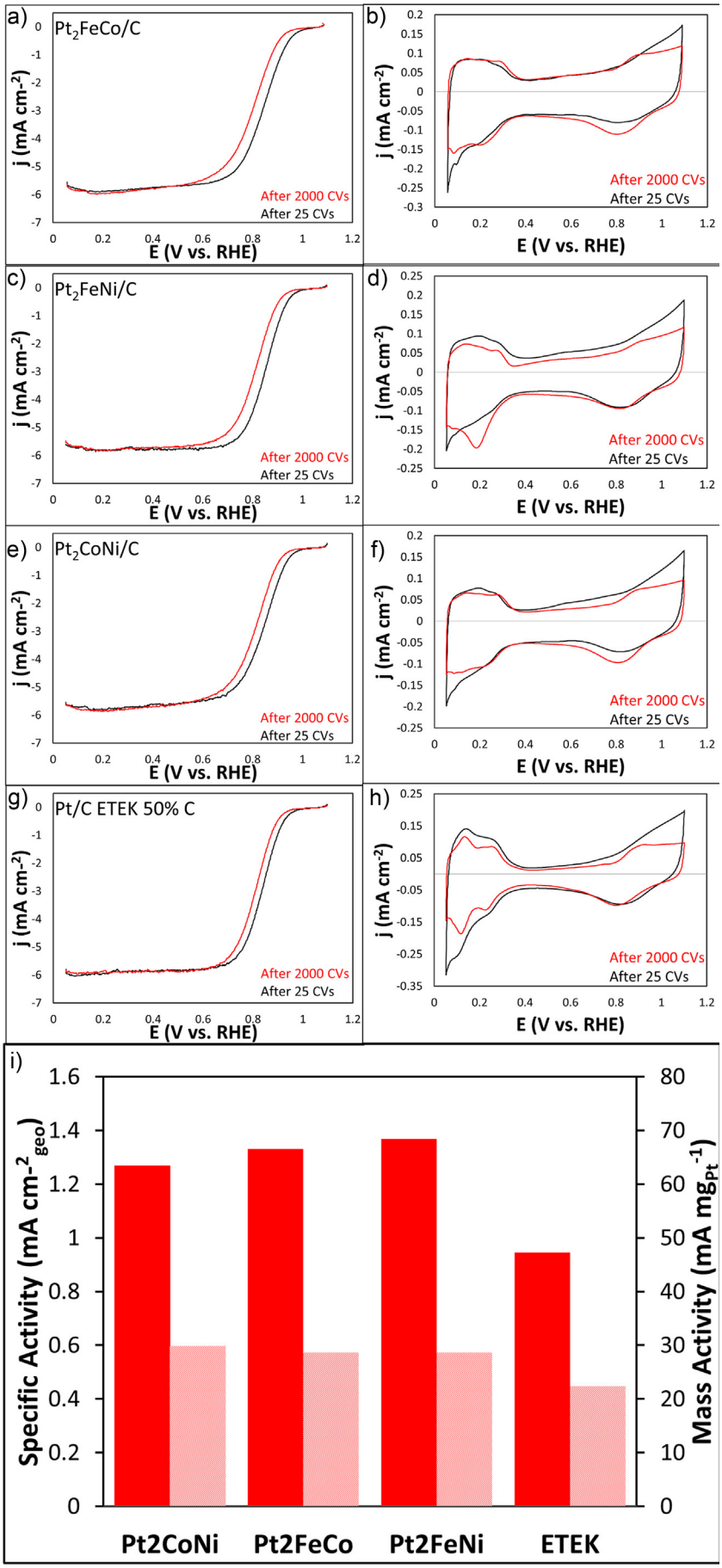
a)
Pt2FeCo/C
j (mA cm-2)
E (V vs. RHE)
After 2000 CVs
After 25 CVs
b)
j (mA cm-2)
E (V vs. RHE)
After 2000 CVs
After 25 CVs
c)
Pt2FeNi/C
j (mA cm-2)
E (V vs. RHE)
After 2000 CVs
After 25 CVs
d)
j (mA cm-2)
E (V vs. RHE)
After 2000 CVs
After 25 CVs
e)
Pt2CoNi/C
j (mA cm-2)
E (V vs. RHE)
After 2000 CVs
After 25 CVs
f)
j (mA cm-2)
E (V vs. RHE)
After 2000 CVs
After 25 CVs
g)
Pt/C ETEK 50% C
j (mA cm-2)
E (V vs. RHE)
After 2000 CVs
After 25 CVs
h)
j (mA cm-2)
E (V vs. RHE)
After 2000 CVs
After 25 CVs
i)
Specific Activity (mA cm-2geo)
Mass Activity (mA mgPt-1)
Pt2CoNi
Pt2FeCo
Pt2FeNi
ETEK

Table 2
Summary of oxygen reduction reaction (ORR) activity of ordered Pt_2FeCo/C, Pt_2FeNi/C, Pt_2CoNi/C, and $Pt/C_{E\text{-}TEK}$ 50 wt% standard. Electrochemical measurements were done in 0.1 M $HClO_4$. The cyclic voltammetry (CV) measurements were done at a rate of 20 mV/s from 0.05 to 1.10 V.

Electrode material	Pt loading ($\mu g/cm^2$)	ECSA (m^2/g_{Pt})		Mass activity @ 0.9 V 20 mV/s (mA/mg_{Pt})		Specific activity @ 0.9 V 20 mV/s ($\mu A/cm^2_{Pt}$)		Half-wave potential − $E_{1/2}$ (V vs. Ag/AgCl)	
		After 25 CVs	After 2000 CVs	After 25 CVs	After 2000 CVs	After 25 CVs	After 2000 CVs	After 25 CVs	After 2000 CVs
Pt_2FeCo/C	20.0	4.51	3.87	66.5	28.6	133	57	0.84	0.80
Pt_2FeNi/C	20.0	4.25	5.12	68.4	28.6	137	57	0.85	0.81
Pt_2CoNi/C	20.0	3.97	3.10	63.4	29.8	127	60	0.84	0.81
$Pt/C_{(ETEK)}$	20.0	7.31	4.96	47.2	22.4	94	45	0.84	0.81

3.3. Particle size analysis

The transmission electron microscopy (TEM) images and the corresponding histograms of Pt_2FeCo/C, Pt_2FeNi/C, and Pt_2CoNi/C annealed at 550 °C are shown in Fig. 5 (Fig. S6 shows them after cycling in 0.1 M H_2SO_4), and particle sizes are tabulated in Table S2. These images show that the Pt-based intermetallics have spherical shape, and are sufficiently distributed over the carbon support; however, while particle agglomeration is reduced significantly using this method, agglomeration is not completely avoidable. The particle size distribution and the total surface area of the intermetallics can be analyzed using different region of the particles from these images. The average diameters of each intermetallic particle were 3–5 nm. The distributions of particle size in the histograms were measured by TEM images for more than 100 particles in each sample.

3.4. ORR activity

The electrochemical behavior of Pt_2FeCo/C, Pt_2FeNi/C, and Pt_2CoNi/C electrocatalysts was examined by cyclic voltammetry and rotating disk electrode (RDE) voltammetry. The platinum electrochemical active surface areas (ECSAs) and the changes in chemical composition of Pt and the 3d transition metals are determined before and after the electrochemical experiments. Fig. 6 shows the ORR polarization curves and the summary of mass and specific activity of all the electrode materials and $Pt/C_{E\text{-}TEK}$ standard after approximately 25 and 2000 cycles in $HClO_4$. Table 2 summarizes the changes in ECSA, mass activity, specific activity, and half-wave potential for ORR of each electrode material after 25 and 2000 cycles in 0.1 M $HClO_4$ (Fig. S7 shows the ORR polarization curves and CVs of Pt_2FeCo/C, Pt_2FeNi/C, Pt_2CoNi/C and 50 wt% $Pt/C_{E\text{-}TEK}$ after 25 and 2000 CV cycles in 0.1 M H_2SO_4, and Table S3 summarizes activity for ORR in 0.1 M H_2SO_4). All of the CVs show typical characteristic features of a pure Pt surface.

The trend in mass and specific activity (taken from ORR polarization curves at 0.9 V vs. RHE) after 25 CV scans is Pt_2FeNi/C > Pt_2FeCo/C > Pt_2CoNi > Pt/C, though all but Pt/C have very similar activity. The trend after 2000 CV scans is similar. The mass and specific activities are not necessarily the best indicators of ORR activity (as they depend on particle size, active surface area, mass loading on the electrode itself). The half-wave potential, $E_{1/2}$, is more relevant. The $E_{1/2}$ of all 4 samples tested are nearly identical (within 20 mV or so; see Table 2), both after 25 CV scans and 2000 CV scans.

3.5. Electrochemical stability

The ordered pseudo-ternary materials are relatively more stable than their alloy counterparts with regard to non-Pt metal leaching. The change in ECSA after stability testing (2000 cycles from 0.05 to 1.10 V at 50 mV/s), suggests a diminution in active surface area by phenomena such as agglomeration or loss of particles, which is comparable to that of the $Pt/C_{E\text{-}TEK}$ standard. Pt_2FeNi shows a curious increase in ECSA, though it is only a small increase. The changes in the half-wave potential of the ordered pseudo-ternary electrode materials before and after stability tests were comparable to that of Pt/C. All four electrode materials showed a decrease of approximately 30 mV.

4. Conclusions

Ordered tetragonal Pt_2FeCo, Pt_2FeNi, and Pt_2CoNi in the 4–6 nm size range were synthesized using a modified solution-phase co-reduction method, which utilizes the KCl byproduct to kinetically stabilize the NPs from agglomeration upon annealing at moderately high temperatures (550 °C). The ordered nanoparticles were transferred onto a carbon support using ethylene glycol and various sonication techniques. The electrode materials were characterized using XRD, EDX, TGA, and TEM to determine the crystal structure, atomic composition, wt% on carbon-black, and particle size. The ORR activity and stability of these nanomaterials were tested in 0.1 M $HClO_4$ and 0.1 M H_2SO_4 using CV and RDE electrochemical techniques. All showed comparable to slightly improved mass and specific activity for ORR compared to the Pt/C 50 wt% ETEK standard.

Acknowledgments

Minh Nguyen carried out the synthesis and initial characterization of the nanoparticles. That part of the project was supported by the Department of Energy office of Basic Energy Sciences through grant DE-FG02-87ER45298. Minghui Yang carried out the Rietveld analysis of X-ray diffraction data and was supported by Cornell funds. Ryo H. Wakabayashi carried out the electrochemical ORR studies and was supported by the Energy Materials Center at Cornell (EMC^2), an Energy Frontier Research Center funded by the U.S. Department of Energy, Office of Science, Office of Basic Energy Sciences, Office of Science, Office of Basic Energy Sciences under Award Number DE-SC0001086. The EDX and TEM measurements were obtained in facilities managed and maintained by the Cornell

Fig. 6. ORR cathodic polarization curves of Pt_2FeCo/C, Pt_2FeNi/C. Pt_2CoNi/C, and $Pt/C_{E\text{-}TEK}$ 50 wt% after 25 CVs (a) (c) (e) (g) respectively, and after 2000 CVs (b) (d) (f) (h), respectively. ORR polarization curves were done in O_2 saturated 0.1 M $HClO_4$ at a rate of 20 mV/s from 1.10 to 0.20 V. CVs were done from 0.05 to 1.10 V at 50 mV/s in N_2 saturated 0.1 M $HClO_4$. (i) ORR activity summary of the ordered pseudo-ternary electrode materials after 25 CVs (solid) and 2000 CVs (dashed) vs. Pt/C 50 wt% Etek standard. For each electrode material, the pink bars indicate the mass activity and the red bars indicate the specific activity. The activity was taken from ORR polarization curves at 0.9 V at a sweep rate of 20 mV/s during the cathodic sweep. The CVs were done from 0.05 to 1.10 V at a sweep rate of 20 mV/s. (For interpretation of the references to colour in this figure legend, the reader is referred to the web version of this article.)

Center for Materials Research (CCMR), an NSF supported MRSEC through Grant DMR-1120296.

Appendix A. Supplementary data

Supplementary data related to this article can be found at http://dx.doi.org/10.1016/j.jpowsour.2015.01.076.

References

[1] K.V. Kordesch, G.R. Simader, Chem. Rev. 95 (1995) 191.
[2] M.K. Debe, Nature 486 (2012) 43.
[3] D. Simonsson, Chem. Soc. Rev. 26 (1997) 181.
[4] B.C.H. Steele, A. Heinzel, Nature 414 (2001) 345.
[5] S. Chu, A. Majumdar, Nature 488 (2012) 294.
[6] M.K. Carpenter, T.E. Moylan, R.S. Kukreja, M.H. Atwan, M.M. Tessema, J. Am. Chem. Soc. 134 (2012) 8535.
[7] Y.H. Bing, H.S. Liu, L. Zhang, D. Ghosh, J.J. Zhang, Chem. Soc. Rev. 39 (2010) 2184.
[8] J.I. Shui, C. Chen, J.C.M. Li, Adv. Funct. Mater. 21 (2011) 3357.
[9] A.C. Chen, P. Holt-Hindle, Chem. Rev. 110 (2010) 3767.
[10] L.F. Yang, S.Y. Shan, R. Loukrakpam, V. Petkov, Y. Ren, B.N. Wanjala, M.H. Engelhard, J. Luo, J. Yin, Y.S. Chen, C.J. Zhong, J. Am. Chem. Soc. 134 (2012) 15048.
[11] D.S. Wang, Y.D. Li, Adv. Mater. 23 (2011) 1044.
[12] A.R. Malheiro, J. Perez, H.M. Villullas, J. Power Sources 195 (2010) 3111.
[13] Y.K. Zhou, K. Neyerlin, T.S. Olson, S. Pylypenko, J. Bult, H.N. Dinh, T. Gennett, Z.P. Shao, R. O'Hayre, Energy Environ. Sci. 3 (2010) 1437.
[14] J. Luo, L.Y. Wang, D. Mott, P.N. Njoki, N. Kariuki, C.J. Zhong, T. He, J. Mater. Chem. 16 (2006) 1665.
[15] J.J. Moore, H.J. Feng, Prog. Mater. Sci. 39 (1995) 275.
[16] T. Trindade, P. O'Brien, N.L. Pickett, Chem. Mater. 13 (2001) 3843.
[17] S.C. Yang, Z.M. Peng, H. Yang, Adv. Funct. Mater. 18 (2008) 2745.
[18] Y. Vasquez, Z.P. Luo, R.E. Schaak, J. Am. Chem. Soc. 130 (2008) 11866.
[19] Y.J. Kang, C.B. Murray, J. Am. Chem. Soc. 132 (2010) 7568.
[20] W. Chen, R. Yu, L.L. Li, A.N. Wang, Q. Peng, Y.D. Li, Angew. Chem. Int. Ed. 49 (2010) 2917.
[21] Y.J. Kang, J.B. Pyo, X.C. Ye, T.R. Gordon, C.B. Murray, ACS Nano 6 (2012) 5642.
[22] D.C. Lee, F.V. Mikulec, J.M. Pelaez, B. Koo, B.A. Korgel, J. Phys. Chem. B 110 (2006) 11160.
[23] J.M. Kim, C.B. Rong, J.P. Liu, S.H. Sun, Adv. Mater. 21 (2009) 906.
[24] C.N.R. Rao, H.S.S.R. Matte, R. Voggu, A. Govindaraj, Dalton Trans. 41 (2012) 5089.
[25] A.C. Larson, R.B. Von Dreele, General Structure Analysis System (GSAS), Los Alamos National Laboratory, 1994. Report LAUR 86-748.
[26] M.H. Yang, M.J. MacLeod, F. Tessier, F.J. DiSalvo, J. Am. Ceram. Soc. 95 (2012) 3084.
[27] N. Markovic, H. Gasteiger, P.N. Ross, J. Electrochem. Soc. 144 (1997) 1591.
[28] U.A. Paulus, T.J. Schmidt, H.A. Gasteiger, R.J. Behm, J. Electroanal. Chem. 495 (2001) 134.
[29] Y. Garsany, O.A. Baturina, K.E. Swider-Lyons, S.S. Kocha, Anal. Chem. 82 (2010) 6321.
[30] E. Clementi, D.L. Raimondi, W.P. Reinhard, J. Chem. Phys. 47 (1967) 1300.
[31] J.C. Woolley, B. Bates, J. Less Common Met. 2 (1960) 11.
[32] G.T. Stevens, M. Hatherly, J.S. Bowles, J. Mater. Sci. 13 (1978) 499.
[33] J.C. Woolley, B. Bates, J. Less Common Met. 1 (1959) 382.
[34] B.E. Warren, X-ray Diffraction, General Publishing Company, 1969.
[35] Y. Xu, A.V. Ruban, M. Mavrikakis, J. Am. Chem. Soc. 126 (2004) 4717.